ECCO: A new approach to estimate the time variability of the Meridional Overturning Circulation in the South Atlantic at 30ºS

Cristina Arumí Planas

2018/2019

Tutor: Alonso Hernández Guerra
Cotutora: María Casanova Masjoan

Trabajo Fin de Título para la obtención del título Graduada en Ciencias del Mar.

ECCO: A new approach to estimate the time variability of the Meridional Overturning Circulation in the South Atlantic at 30^{o}S

by

Cristina Arumí Planas

Submitted in fulfilment of the requirements for:
GRADO EN CIENCIAS DEL MAR
at
UNIVERSIDAD DE LAS PALMAS DE GRAN CANARIA

Signature of Author……Cristina Arumí Planas……..
FACULTAD DE CIENCIAS DEL MAR
UNIVERSIDAD DE LAS PALMAS DE GRAN CANARIA

Signature of Tutor……Alonso Hernández Guerra……..
INSTITUTO DE OCEANOGRAFÍA Y CAMBIO GLOBAL
DEPARTAMENTO DE FÍSICA
FACULTAD DE CIENCIAS DEL MAR
UNIVERSIDAD DE LAS PALMAS DE GRAN CANARIA

Signature of co-Tutor……María Casanova Masjoan……..
INSTITUTO DE OCEANOGRAFÍA Y CAMBIO GLOBAL
DEPARTAMENTO DE FÍSICA
FACULTAD DE CIENCIAS DEL MAR
UNIVERSIDAD DE LAS PALMAS DE GRAN CANARIA

Las Palmas de Gran Canaria, July 2019

TABLE OF CONTENTS

ABSTRACT

Time series of mass transport for the upper, deep and abyssal layers in the Atlantic Ocean at 30ºS have been estimated using data obtained from the ECCOv4r3, a model developed by the Jet Propulsion Laboratory under a contract with the NASA. These estimations have been compared with analogous data obtained from the GO-SHIP hydrographic transoceanic sections at 30ºS from 1993, 2003 and 2011. Results show that the ECCOv4r3 solution for the upper layers (γ^n<27.58 kg/m^3) is not significantly different from the mass transports estimated by the hydrographic data. This is not the case, however, for the deep and abyssal layers (γ^n>27.58 kg/m^3), where noticeable differences are found. The ECCOv4r3 points out that the Brazil Current shows a seasonal variability with higher mass transport from August to March (-15.8±0.7 Sv) than from April to July (-13.3±0.4 Sv). Furthermore, the ECCOv4r3 indicates that the Benguela Current shows a seasonal variability with higher mass transport from June to November (13.8±0.3 Sv) than from December to May (13.1±0.2 Sv). The comparison of heat transport and freshwater flux estimated with ECCOv4r3 to those obtained from hydrographic data show no significant differences. Nevertheless, the freshwater flux estimated by hydrographic data suggest that it has been decreasing during the study period, while the same estimation with ECCOv4r3 data do not show any decrease. The overturning stream-function estimated with ECCOv4r3 is not significantly different than the AMOC estimated by hydrographic data for the thermocline and intermediate layers. The ECCOv4r3 reveals that the AMOC shows a seasonal variability with stronger mass transport from April to September (16.6±0.9 Sv) than from October to March (14.5±0.2 Sv).

1. INTRODUCTION

The World Ocean Circulation Experiment (WOCE) was a global oceanographic research program dealing with long-term variability in ocean circulation, property distributions, and their relation to climate. One of the main objectives of the WOCE was the estimation of oceanic transport of water mass, heat, and freshwater as well as the mixing of surface waters to the seafloor of each ocean using hydrographic data from zonal and meridional sections of closely spaced stations (Chapman, 1998; Ganachaud and Wunsch, 2003; Ganachaud, 2003; Macdonald and Hole, 1996).

The Meridional Overturning Circulation (MOC) is a variable-in-time three-dimensional system based on all the ocean basins, including the Atlantic Ocean (Gordon, 1986; Lumpkin and Speer, 2007; Talley, 2003). The Atlantic Ocean is a unique feature within the Earth's climate system as it is the only ocean where currents, driven by differences in temperature and salt content, transport net heat from the Southern Hemisphere across the equator toward the northern subpolar gyre. This system of ocean currents is the Atlantic Meridional Overturning Circulation (AMOC). Firstly, the AMOC transports surface and intermediate waters northward, where they lose heat to the atmosphere, become cooler and denser, and subsequently sink and form deep water in the Labrador and Nordic Seas. Secondly, water masses return southward, mainly along the Deep Western Boundary Current (DWBC), to the tropical and southern Atlantic, where they interact with waters that originated around the continental shelf of Antarctica and are then exported to the Indian and Pacific Oceans (Dickson and Brown, 1994; Volkov et al., 2019). The main gateways for the entrainment of surface and intermediate waters from the Indian and Pacific basins into the surface waters of the South Atlantic Ocean are the Drake Passage and the Agulhas Retroflection Regions (Stramma and England, 1999).

According to the procedure established in WOCE, horizontal sampling of the different ocean properties is collected by high accuracy measurements from the sea surface to the seafloor with an approximate decadal base, a spatial resolution related to the internal Rossby radius and sections that extend from coast to coast or enclosed regions (Hernández-Guerra et al., 2019). The insufficient spatial and temporal samplings produce a distortion of the original signal, referred to in the literature as aliasing. Aliasing is a well-known oceanographic problem that needs to be faced, for instance, to identify ocean circulation features such as synoptic eddies, internal waves, etc. (Bretherton et al., 1976; Cushman-Roisin and Beckers, 2007; Talley, 2003; Thiébaux and Pedder, 1987; Wunsch, 1996). In order to minimize the aliasing effects over time, the Jet Propulsion Laboratory of the California Institute of Technology under a contract with the National Aeronautics and Space Administration (NASA) have developed ECCOv4r3 (Estimating the Circulation and Climate of the Ocean Version 4 Release 3). ECCOv4r3 is an enhanced model that includes monthly data of the state of the ocean's evolution over time for the time period 1992-2015 (Forget et al., 2015; Fukumori et al., 2017).

The main goal of this study is to assess the reliability and representativeness of ECCOv4r3 results. In order to accomplish this objective, results from the ECCOv4r3 model in the South Atlantic Ocean at 30ºS are compared with results from research

studies that performed estimations of the circulation in the years 1993, 2003 and 2011 (Ganachaud, 2003; Hernández-Guerra et al., 2019). The second objective consists of estimating the time variability of the AMOC, the Brazil and Benguela Currents, the heat transport and the freshwater flux in the South Atlantic Ocean at 30ºS using the whole period of ECCOv4r3 data.

This study is organized as follows: section 2 presents the data collection and the vertical sections of different ocean properties. Section 3 presents θ/S diagrams for 1993, 2003 and 2011, the accumulated mass transport for the upper, deep and abyssal layers, the seasonal and interannual variability of Brazil and Benguela Currents, heat transport and freshwater flux, and for the AMOC. Finally, section 4 gives a discussion with conclusive remarks.

2. DATA AND METHODS

ECCOv4r3 represents the latest ocean state estimate of the Consortium for Estimating the Circulation and Climate of the Ocean (ECCO) (Wunsch and Heimbach, 2013; Wunsch et al., 2009). According to Fukumori et al. (2017), ECCOv4r3 synthesizes a general ocean circulation model and produces a physical description of the state of the ocean's evolution over time. The data feeding this model include satellite altimetry (Sea Surface Height, SSH), Gravity Recovery and Climate Experiment (GRACE) with modelled Ocean Bottom Pressure (OBP), Advanced Very High-Resolution Radiometer (AVHRR) Sea Surface Temperature (SST), Aquarius Sea Surface Salinity (SSS), Argo, Conductivity Temperature Depth (CTD), Expandable Bathythermograph (XBT), mooring temperature and salinity data, sea-ice measurements, and global mean SSH and OBP. The ECCOv4r3 model estimates the ocean state by using the adjoint method to iteratively minimize the squared sum of weighted model-data misfits and control adjustments (Wang et al., 2017). The main results of the last ECCOv4 release are available through the Jet Propulsion Laboratory, California Institute of Technology, under a contract with the NASA (ftp://ecco.jpl.nasa.gov/Version4/Release3/).

As stated in Wang et al. (2017), the ECCOv4r3 model splits the globe into 13 regional tiles, of which only tiles 2 and 12 are used for this study (Figure 1). For these tiles, data covering the period from January 1992 through December 2015 have been used, which cover the entire water column of 67 selected stations located in the South Atlantic Ocean at 30ºS (Figure 2). In order to assess the reliability and

representativeness of ECCOv4r3 results, they are compared to hydrographic data along section A10, nominally at 30ºS in the South Atlantic Ocean, available through the Carbon Hydrographic Data Office (CCHDO, http://cchdo.ucsd.edu). Specifically, mass transport in section A10 has been previously computed by Ganachaud (2003) in January 1993, and by Hernández-Guerra et al. (2019) in November 2003 and October 2011, which in this case it has been computed with estimations from ECCOv4r3. The data used to accomplish this objective for 2003 and 2011 are hydrographic data computed using Model C, which is the 'classic' inverse model explained in Hernández-Guerra et al. (2019), as it resembles more the model used by Ganachaud (2003) to compute the data for 1993.

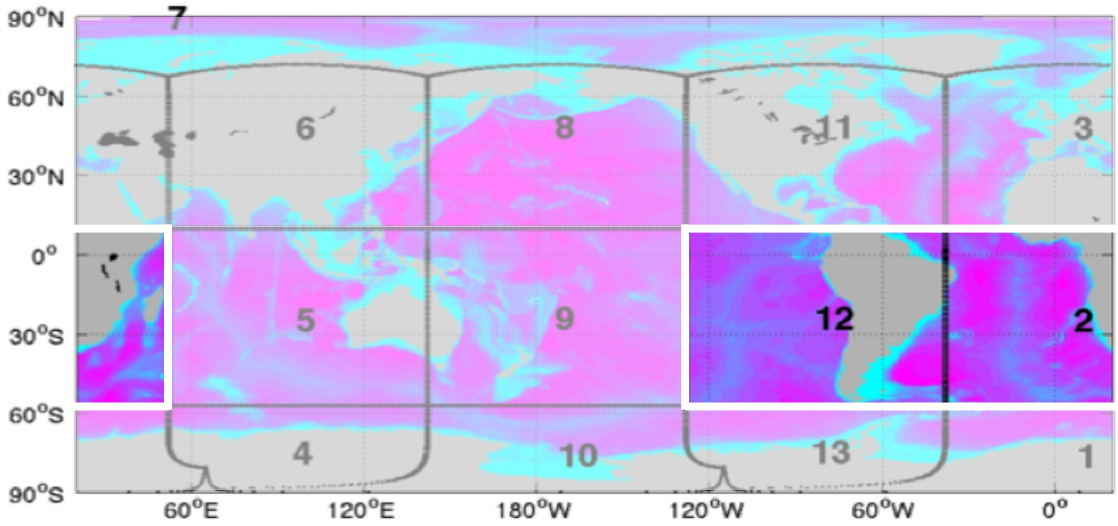

Figure 1. The partitioning of the globe into 13 regional tiles (modified from Wang et al., 2017).

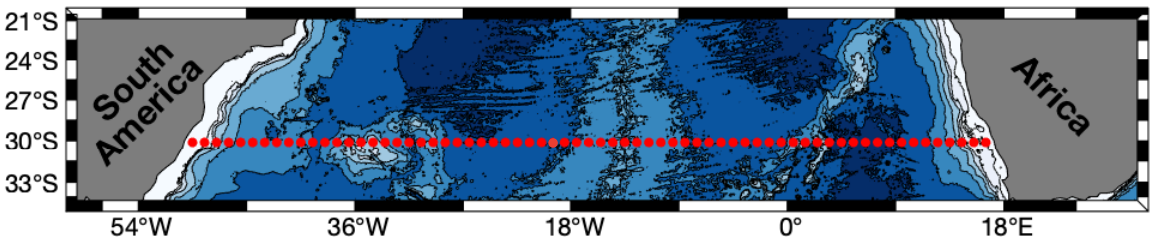

Figure 2. ECCO selected station positions in the South Atlantic Ocean at 30ºS.

Transatlantic vertical sections of potential temperature, salinity, neutral density, and oxygen are shown in figures 3-6 and are used to identify the existing water masses, following Talley et al. (2011). Vertical sections of potential temperature, salinity, and neutral density are plotted using ECCOv4r3 data, while the vertical section of oxygen is taken from Hernández-Guerra et al. (2019), since oxygen data are not included in ECCOv4r3 model.

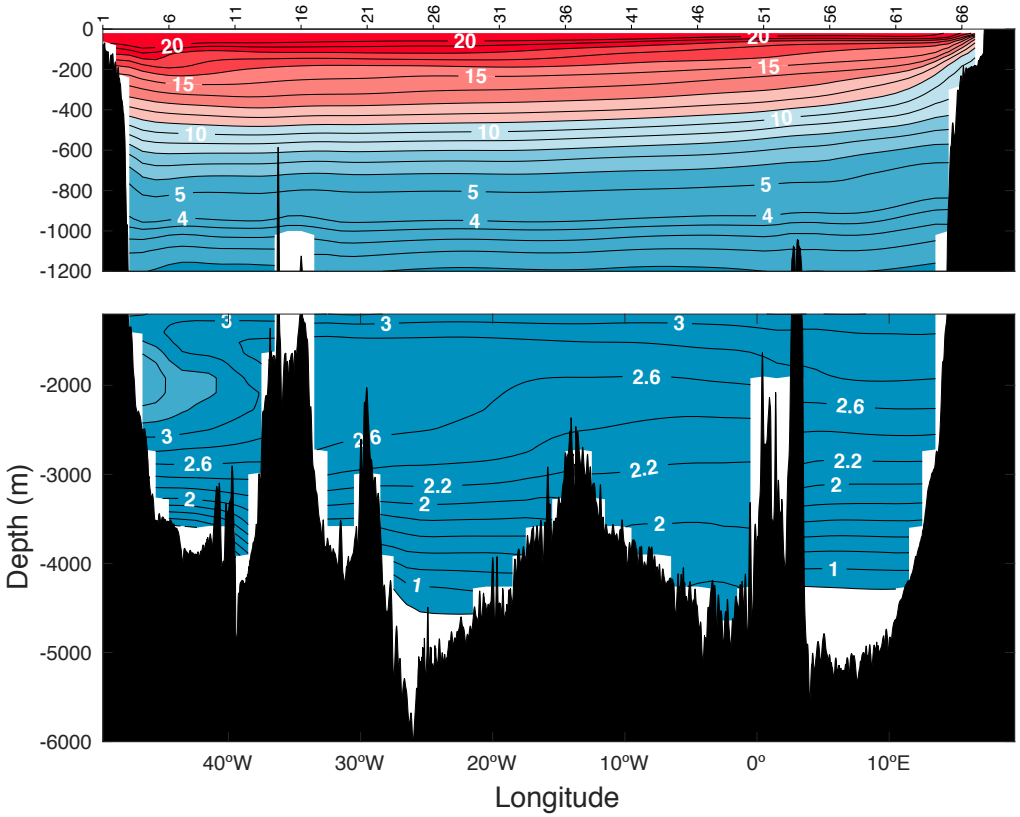

Figure 3. Vertical section of potential temperature (ºC) at 30ºS in the Atlantic Ocean for ECCOv4r3 data collected in January 1992. Ticks on the top axis indicate the location of the stations.

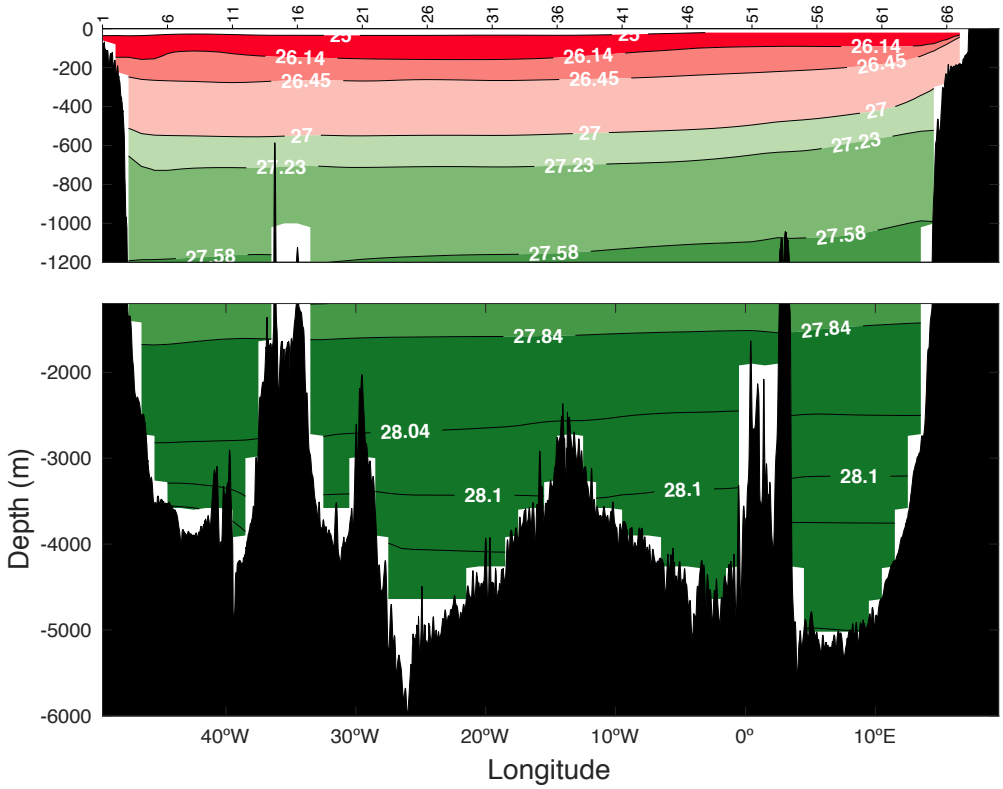

Figure 4. Vertical section of neutral density (γ^n) at 30ºS in the Atlantic Ocean for ECCOv4r3 data collected in January 1992. Ticks on the top axis indicate the location of the stations.

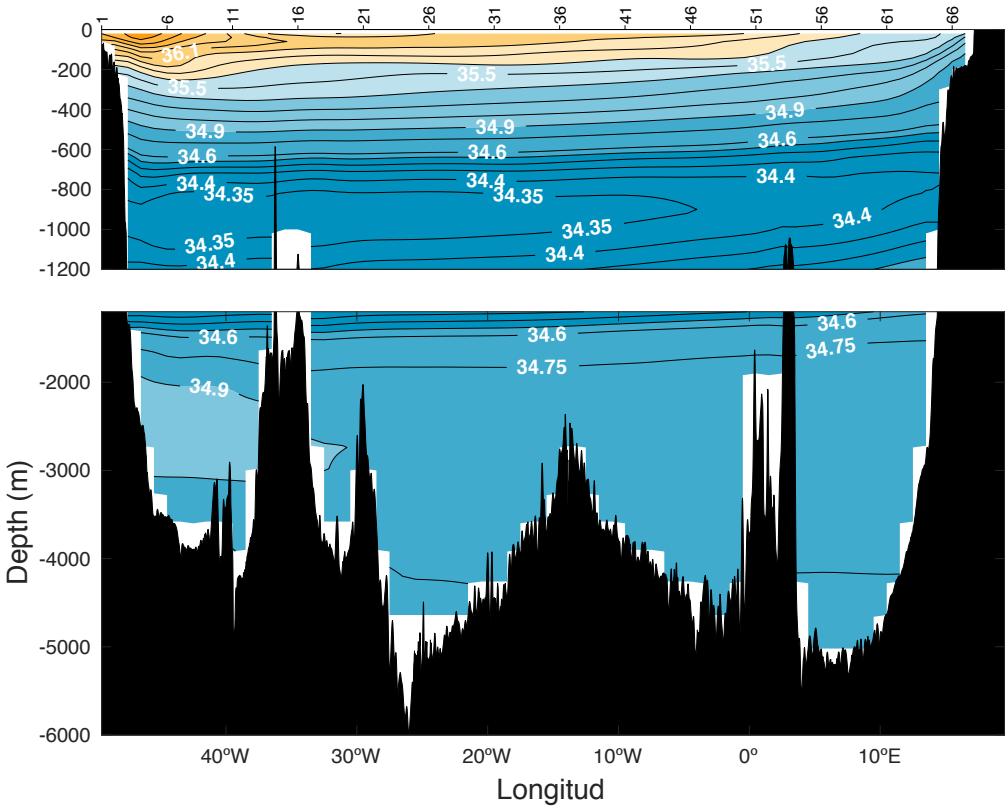

Figure 5. Vertical section of salinity at 30ºS in the Atlantic Ocean for ECCOv4r3 data collected in January 1992. Ticks on the top axis indicate the location of the stations.

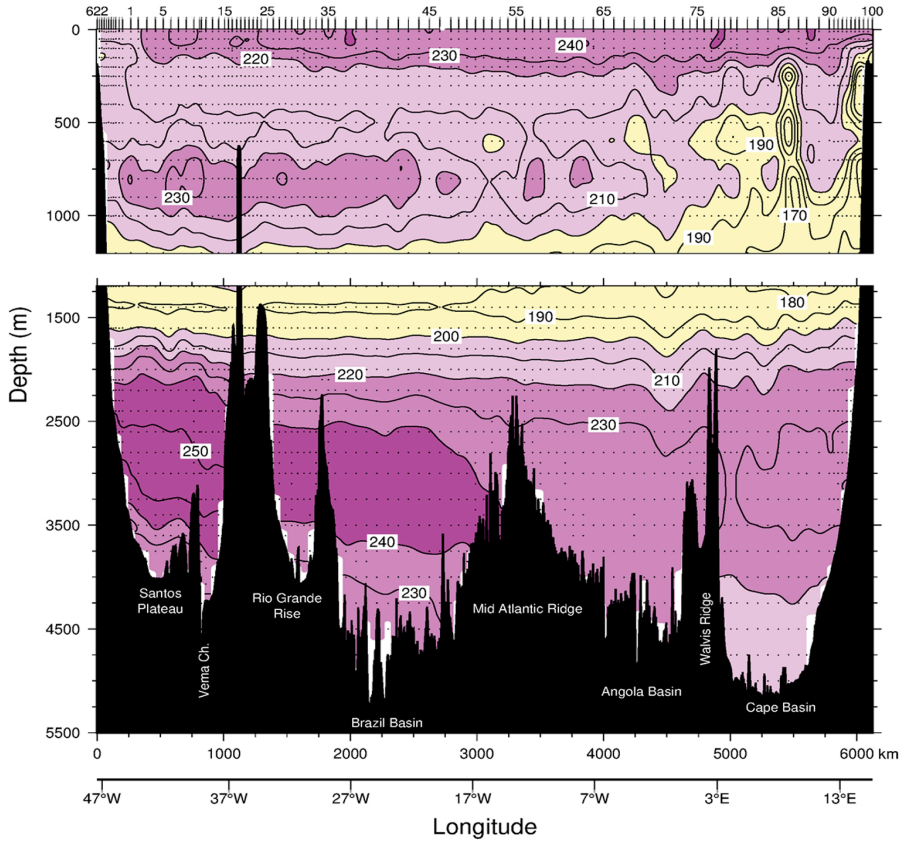

Figure 6. Vertical section of oxygen ($\mu M/kg$) at 30ºS in the Atlantic Ocean for 2003 (from Hernández-Guerra et al., 2019). Ticks on the top axis indicate the location of the stations.

In the upper layer, between the surface and γ^n=27.23 kg/m^3 (above ~730 m) with high salinity values, the South Atlantic Central Water (SACW) is found, which is characterized with subtropical thermocline waters formed by subduction in the subtropical gyre of the South Atlantic Ocean, north of the subtropical front (Gordon, 1981, 1989; Sprintall and Tomczak, 1993).

Below this layer, in the intermediate layers (between 27.23 kg/m^3< γ^n <27.58 kg/m^3), that corresponds to ~730-1140 m, the Antarctic Intermediate Water (AAIW) is located, which is formed by advection of fresh Subantarctic Surface Water (SASW) and characterized by the minimum salinity values (<34.5).

According to Talley et al. (2011), the mixture of Indian Deep Water (IDW), Pacific Deep Water (PDW) and deep waters of the Southern Ocean form the Upper Circumpolar Deep Water (UCDW), with a neutral density range of 27.58 kg/m^3< γ^n<27.84 kg/m^3, extending about 1140-1560 m depth. The UCDW is characterized in the vertical domain by low levels of oxygen (<200 μM/kg) and salinity values in the range 34.3-34.7.

The North Atlantic Deep Water (NADW), located between 27.84 kg/m^3< γ^n <28.1 kg/m^3 from about 1560 to 3400 m depth, is composed of the Upper North Atlantic Deep Water (UNADW), primarily formed by Labrador Sea Waters (Talley and McCartney, 1982) and by the Lower North Atlantic Deep Water (LNADW), with overflow waters from the Nordic Sea (Pickart, 1992; Smethie et al., 2000). The NADW is characterized in the vertical domain by a salinity range of 34.6-34.9 and relatively high oxygen (>240 μM/kg).

The densest water mass, γ^n>28.1 kg/m^3 from approximately 3400 m depth to the seafloor, is called Antarctic Bottom Water (AABW). According to Talley et al. (2011), this water mass is formed by brine rejection in the Southern Ocean, mixed with NADW, PDW and IDW, and characterized in the vertical to be fresher and to have less oxygen than NADW.

Furthermore, the rising isotherms and isoneutrals in the transatlantic vertical sections allow us to identify the effect of the Brazil and Benguela Currents in the western and eastern basins, respectively (Figures 3-5). The Brazil Current is a relatively narrow western boundary current, flowing southward along the coast of South America from about 9ºS to about 38ºS. The Benguela Current is a relatively wide eastern boundary current, flowing northward along the east coast of Africa from approximately 35ºS to 14ºS (Talley et al., 2011).

3. RESULTS

3.1 θ/S diagrams

Figure 7 shows a comparison of the θ/S diagrams from ECCOv4r3 data and those obtained from hydrographic data for (a) January 1993, (b) November 2003 and (c) October 2011 (computed by Ganachaud, 2003 and Hernández-Guerra et al., 2019). According to figure 7, there is high scattering near the surface potential temperature and salinity values, regardless of the year. The different water masses are identified following the descriptions in Section 2. The θ/S diagrams using ECCOv4r3 data are similar to those obtained from hydrographic data for each year, thus suggesting that the ECCOv4r3 model has not created false water masses and contains all the structural characteristics that are persistently and recurrently found in the South Atlantic at 30ºS.

3.2 Accumulated Mass Transport

Figure 8 shows a comparison of the accumulated mass transports for (a) upper (1-5), (b) deep (6-9) and (c) abyssal (10-11) layers from ECCOv4r3 data and hydrographic data for January 1993, November 2003 and October 2011 (computed by Ganachaud, 2003 and Hernández-Guerra et al., 2019). Positive values of accumulated mass transport indicate a northward transport, while negative values indicate a southward transport. This figure shows that the upper and the abyssal layers have a net northward transport, while the deep layers experience a net southward transport. As seen in table 1, the estimated water mass transport for the upper layers with ECCOv4r3 are similar to hydrographic data results in 1993, 2003 and 2011. However, noticeable differences are found in the deep and abyssal layers in 1993, 2003 and 2011, suggesting that ECCOv4r3 is only valid for the upper layers (Table 1).

Table 1. Net mass transport and uncertainty (Sv) for the upper layers flowing to the north, deep layers flowing to the south and abyssal layers flowing to the north for hydrographic data (HD) and ECCOv4r3 (ECCO) data in 1993, 2003 and 2011.

	Mass Transport (Sv)					
Layers	**1993**		**2003**		**2011**	
	HD	**ECCO**	**HD**	**ECCO**	**HD**	**ECCO**
Upper	18±3	15.1±0.3	13.4±0.9	13.6±0.5	16.3±1.4	15.2±0.9
Deep	-23±3	-10.6±0.7	-20.7±3.8	-10.2±1.3	-25.4±4.2	-10.5±0.8
Abyssal	6±1.3	-1.1±0.7	6.5±1.9	-1±0.4	8.3±2.1	-1.5±0.1

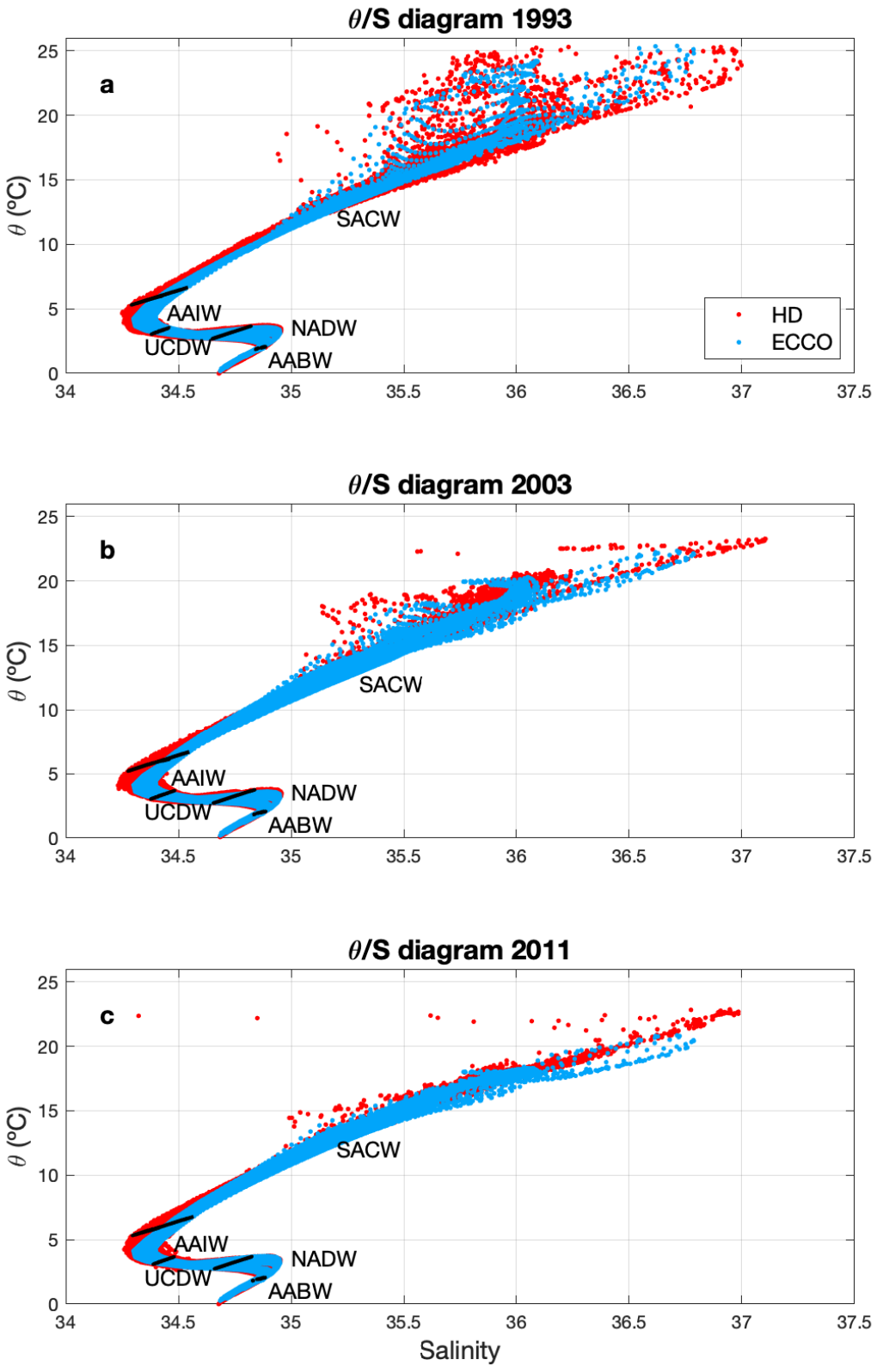

Figure 7. θ/S diagrams used to identify water masses in the Atlantic Ocean at 30ºS in (a) 1993, (b) 2003 and (c) 2011. Red dots represent the results from hydrographic data, and blue dots represent the results with ECCOv4r3 data in South Atlantic at 30ºS. The water masses identified are: South Atlantic Central Water (SACW), Antarctic Intermediate Water (AAIW), Upper Circumpolar Deep Water (UCDW), North Atlantic Deep Water (NADW) and Antarctic Bottom Water (AABW). These waters masses are delimited by the layers of γ^n illustrated with black lines.

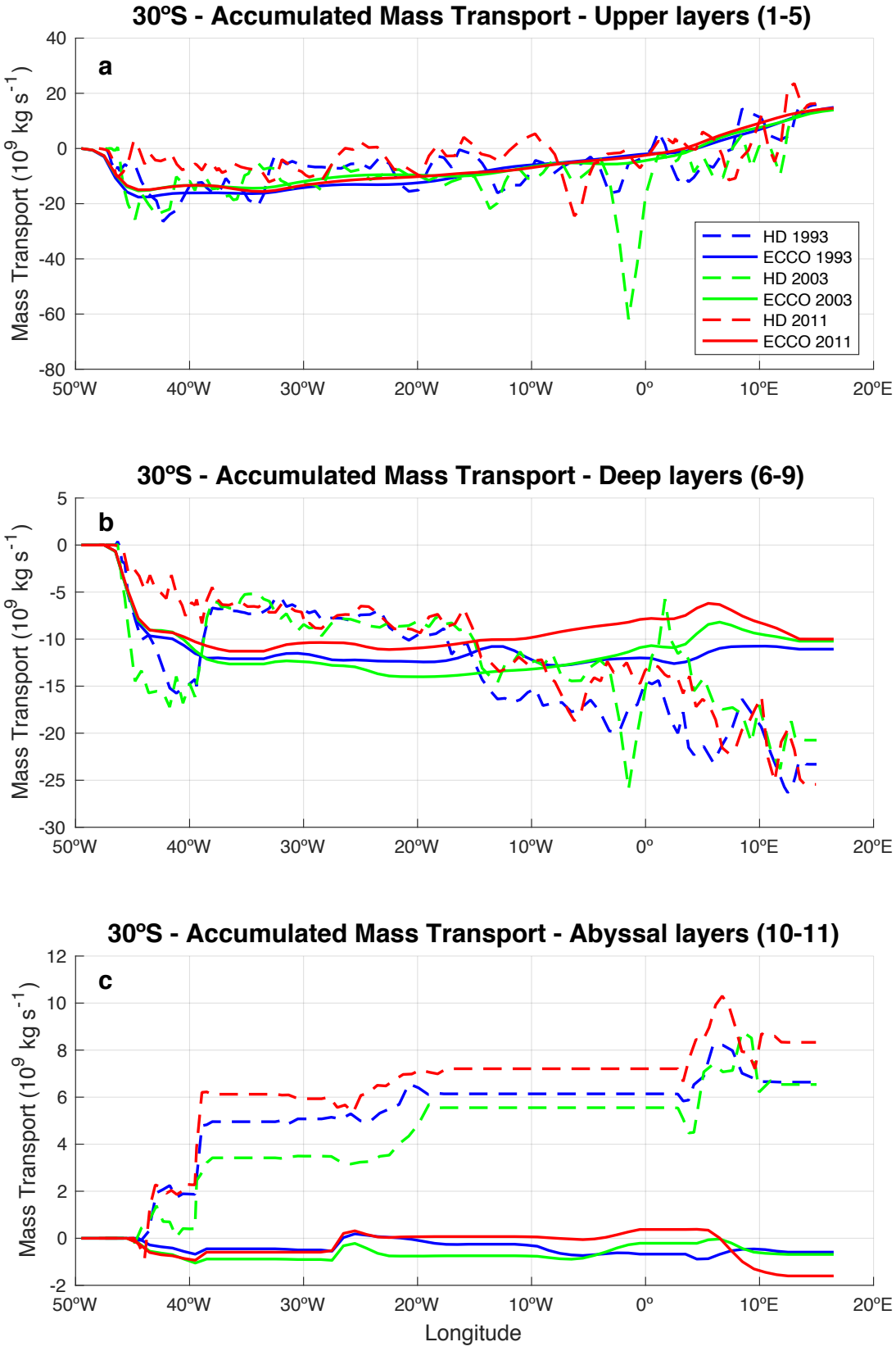

Figure 8. Accumulated mass transport (Sv) at 30ºS for (a) upper, (b) deep and (c) abyssal layers from ECCOv4r3 data (solid lines) and from hydrographic data (dashed lines) for 1993 (blue), 2003 (green) and 2011 (red).

3.3 Brazil and Benguela Currents

Figure 9 shows the seasonal variability of mass transport in the Atlantic Ocean at 30ºS for the (a) Brazil and (b) Benguela Currents. This figure has been generated by using monthly data from the ECCOv4r3 model for the period 1992-2015. The mass transport for the Brazil Current is estimated accumulating the mass transport from the western margin to the location presenting the maximum transport to the south, located at approximately 45ºW. On the other hand, the mass transport for the Benguela Current is estimated accumulating the mass transport from the point where there is a change in the slope of the mass transport (located at around 3ºE) to the eastern margin. Positive values of mass transport indicate a northward transport, while negative values indicate southward transport. The Brazil Current presents higher southward mass transport from August to March (-15.8±0.7 Sv), and weaker southward mass transports from April to July (-13.3±0.4 Sv). The Benguela Current presents higher northward mass transports from June to November (13.8±0.3 Sv) and weaker from December to May (13.1±0.2 Sv).

Analogously, figure 10 shows the interannual variability of mass transport for the (a) Brazil and (b) Benguela Currents in the Atlantic Ocean at 30ºS. Similar to figure 9, this figure is generated from data obtained by the ECCOv4r3 model for the period 1992-2015, but it includes mass transports estimated from hydrographic data for 1993, 2003 and 2011 (computed by Ganachaud, 2003 and Hernández-Guerra et al., 2019). This figure suggests that the southward mass transports for the Brazil Current and northward mass transports for the Benguela Current have been fluctuating across this period without showing any apparent pattern. Furthermore, as seen in table 2, the estimations of the mass transport for the Brazil and Benguela Currents with ECCOv4r3 are significantly different from the mass transports estimated by hydrographic data, with the exception of 1993.

Table 2. Mass transports and uncertainty (Sv) for the Brazil and Benguela Currents for hydrographic data and ECCOv4r3 data in 1993, 2003 and 2011.

	Mass Transport (Sv)			
	Brazil Current		**Benguela Current**	
Año	**HD**	**ECCO**	**HD**	**ECCO**
1993	-14±4	-17.8±0.3	14±2	12±0.3
2003	-25.7±0.7	-15.4±0.0	17.5±0.9	15±0.1
2011	-10.3±0.7	-14.9±0.1	12.2±0.8	14.9±0.1

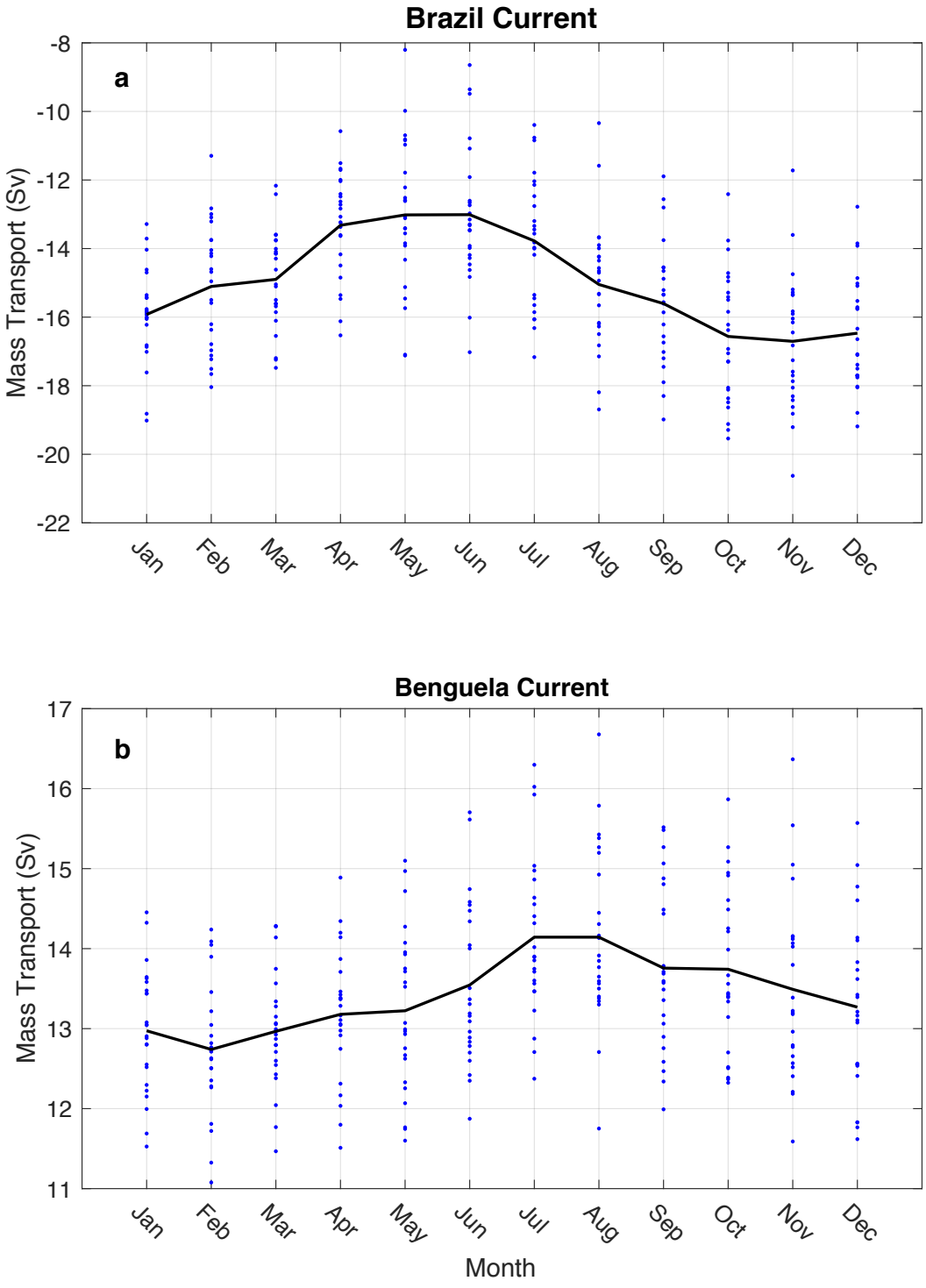

Figure 9. Seasonal variability of mass transport in the Atlantic Ocean at 30ºS for the (a) Brazil and (b) Benguela Currents using ECCOv4r3 data for the period 1992-2015. For each month, the blue dots correspond to the mass transport for each one of the years in the time period considered herein. The black solid line connects the mean mass transport value of each month, averaged by the different years.

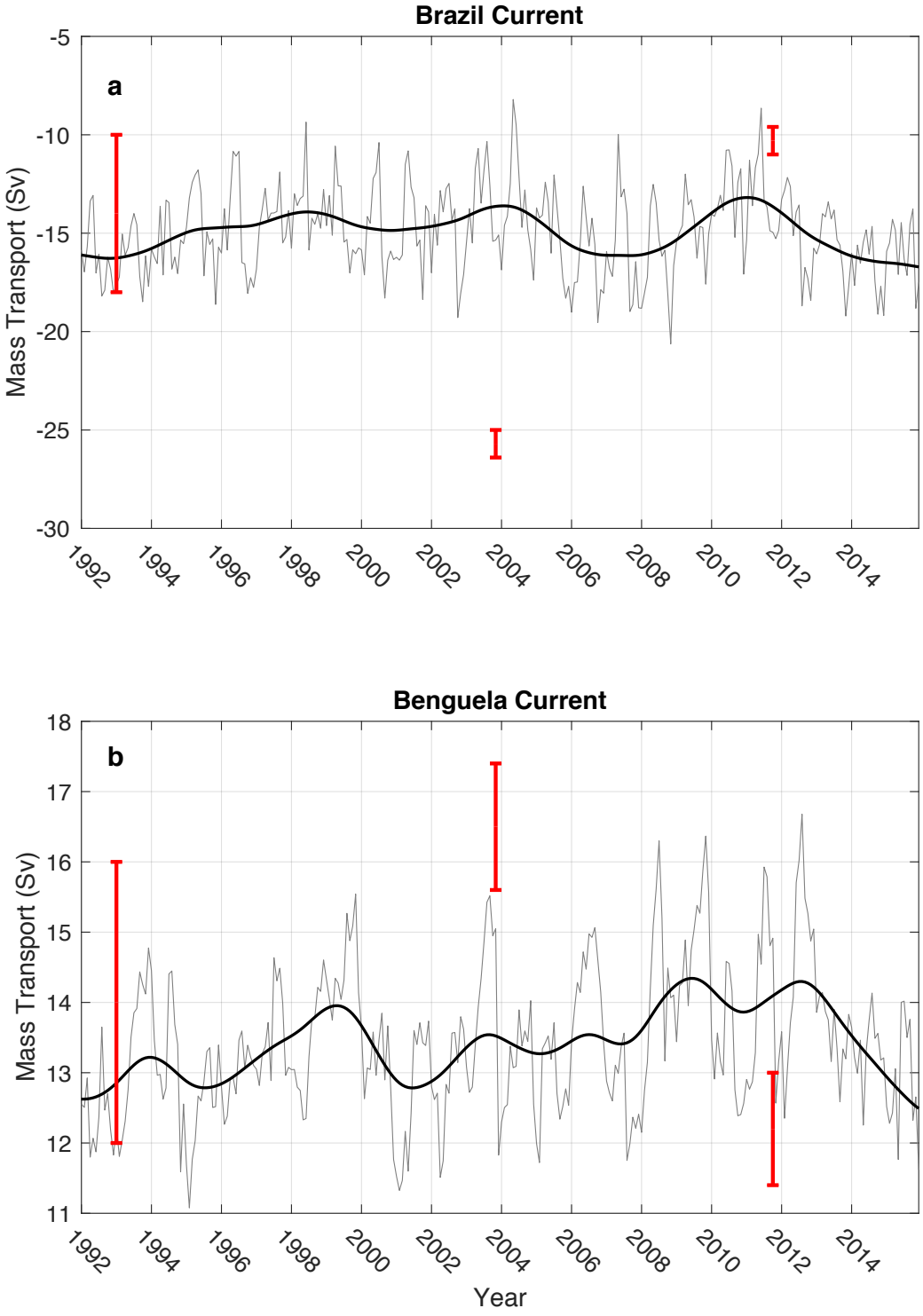

Figure 10. Interannual variability of mass transport corresponding to the (a) Brazil and (b) Benguela Currents for the Atlantic Ocean at 30ºS using ECCOv4r3 data for the period 1992-2015 (grey line), with the Butterworth filter (black line) and mass transport values for Brazil and Benguela Currents obtained from hydrographic data (red error bars) for the years 1993, 2003 and 2011.

3.4 Heat Transport and Freshwater Flux

Heat transport can be computed by using the following expression:

$$T = \sum_i \sum_j \rho_{ij} C_{p_{ij}} \theta_{ij} v_{ij} \, \Delta x \, \Delta z$$

where ρ_{ij} is the density, $C_{p_{ij}}$ is the heat capacity of sea water, θ_{ij} is the potential temperature, v_{ij} the absolute cross-section velocity and i,j are the station pair and layer, respectively. Positive values of heat transport indicate a northward flux, while negative values indicate a southward flux.

Freshwater flux can be computed according to the following expression (Joyce et al., 2001):

$$\bar{F} = \sum_i \sum_j T_{ij} S'_{ij} / S_0$$

where T_{ij} is the absolute mass transport in layer i at station pair j, S'_{ij} is the anomaly of salinity and S_0 the mean salinity (34.9 used by Talley 2008). Positive values of freshwater flux are caused by higher precipitation than evaporation, hence freshwater flux from the atmosphere to the ocean. Negative values of freshwater flux are caused by higher evaporation than precipitation, hence freshwater flux from the ocean to the atmosphere.

Figure 11 shows the seasonal variability of (a) heat transport and (b) freshwater flux in the Atlantic Ocean at 30ºS. This figure has been generated using monthly data from the ECCOv4r3 model for the period 1992-2015. The positive values in figure 11a show that in this area there is a northward flux of heat transport during all year, having stronger northward flux of heat transport from April to September (0.55$\pm$0.07 PW), while from October to March there is a weaker northward flux of heat transport (0.37$\pm$0.01 PW). The negative values in figure 11b show that in this area there is higher evaporation than precipitation for almost all year, presenting higher evaporation from October to March (-0.14$\pm$0.01 Sv) and lower from April to September (-0.03$\pm$0.04 Sv).

Figure 12 shows the interannual variability of (a) heat transport and (b) freshwater flux in the Atlantic Ocean at 30ºS. Similar to figure 11, it is generated by data obtained from the ECCOv4r3 model for the period 1992-2015, and includes heat transports and freshwater fluxes estimated by hydrographic data for the years 1993, 2003 and 2001 (computed by Ganachaud, 2003 and Hernández-Guerra et al., 2019).

Figure 12a suggests that heat transport has similar positive values during the time period of the study, hence having northward flux of heat transport. However, figure 12b suggests that freshwater flux has similar negative values during the time period considered herein, and not decreasing values as supposed in previously published hydrographic data results. Furthermore, as seen in table 3, the estimations with ECCOv4r3 model are not significantly different than the heat transport and freshwater flux estimated by the hydrographic data, except for the freshwater flux in 1993.

Table 3. Heat transport (PW) and freshwater flux (Sv) and its uncertainty for hydrographic data and ECCOv4r3 data in 1993, 2003 and 2011.

	Heat transport (PW)		**Freshwater flux (Sv)**	
Año	**HD**	**ECCO**	**HD**	**ECCO**
1993	0.33±0.08	0.42±0.01	-0.19±0.03	-0.11±0.00
2003	0.34±0.07	0.36±0.04	-0.10±0.03	-0.13±0.03
2011	0.49±0.08	0.44±0.05	0.00±0.04	-0.08±0.05

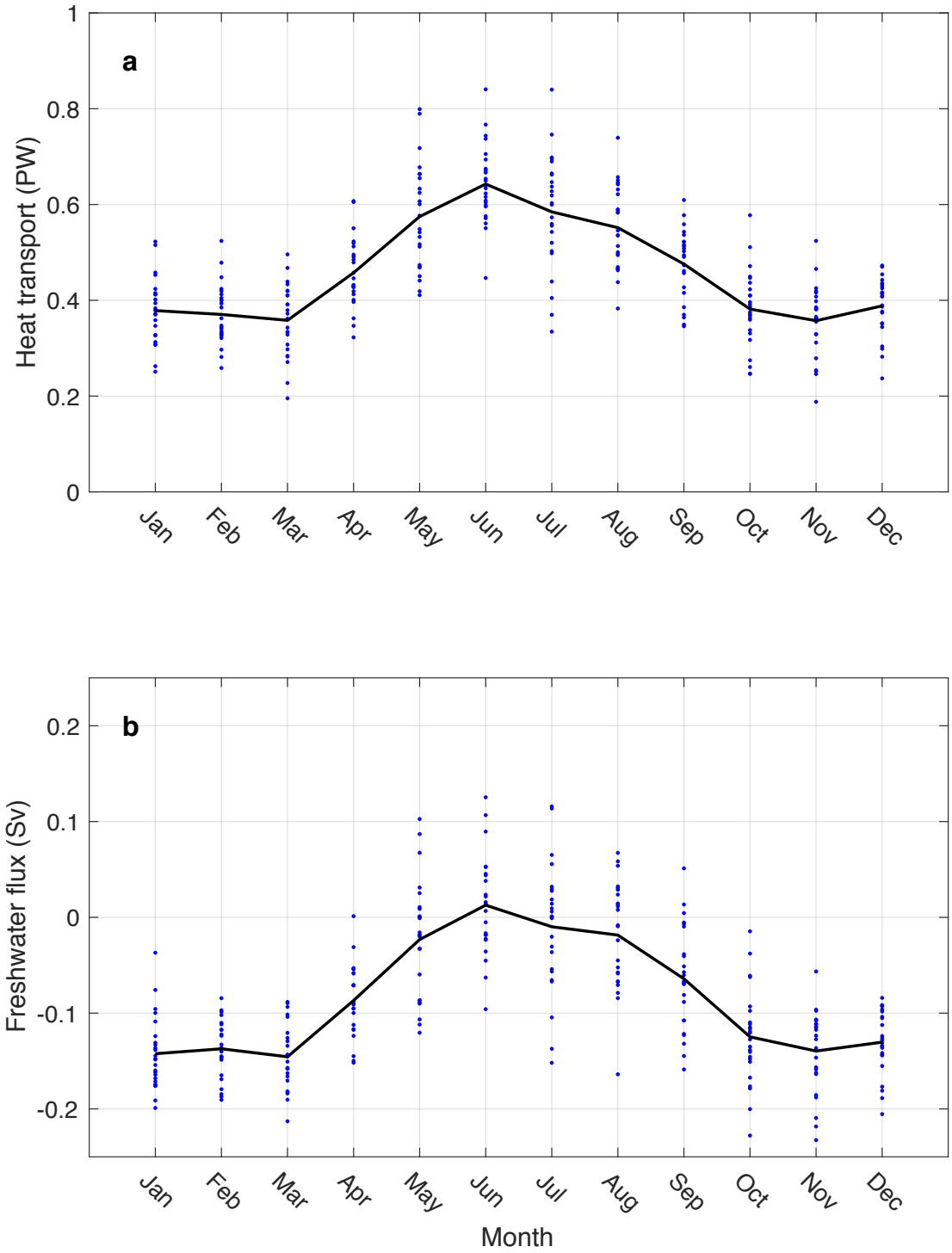

Figure 11. (a) Heat transport (PW) and (b) freshwater flux (Sv) of the South Atlantic at 30ºS for the different months using ECCOv4r3 data for the period 1992-2015. For each month, the blue dots correspond to the heat transport and freshwater flux for each one of the years in the time period considered herein. The black solid line connects the mean heat transport and freshwater flux value of each month, averaged by the different years.

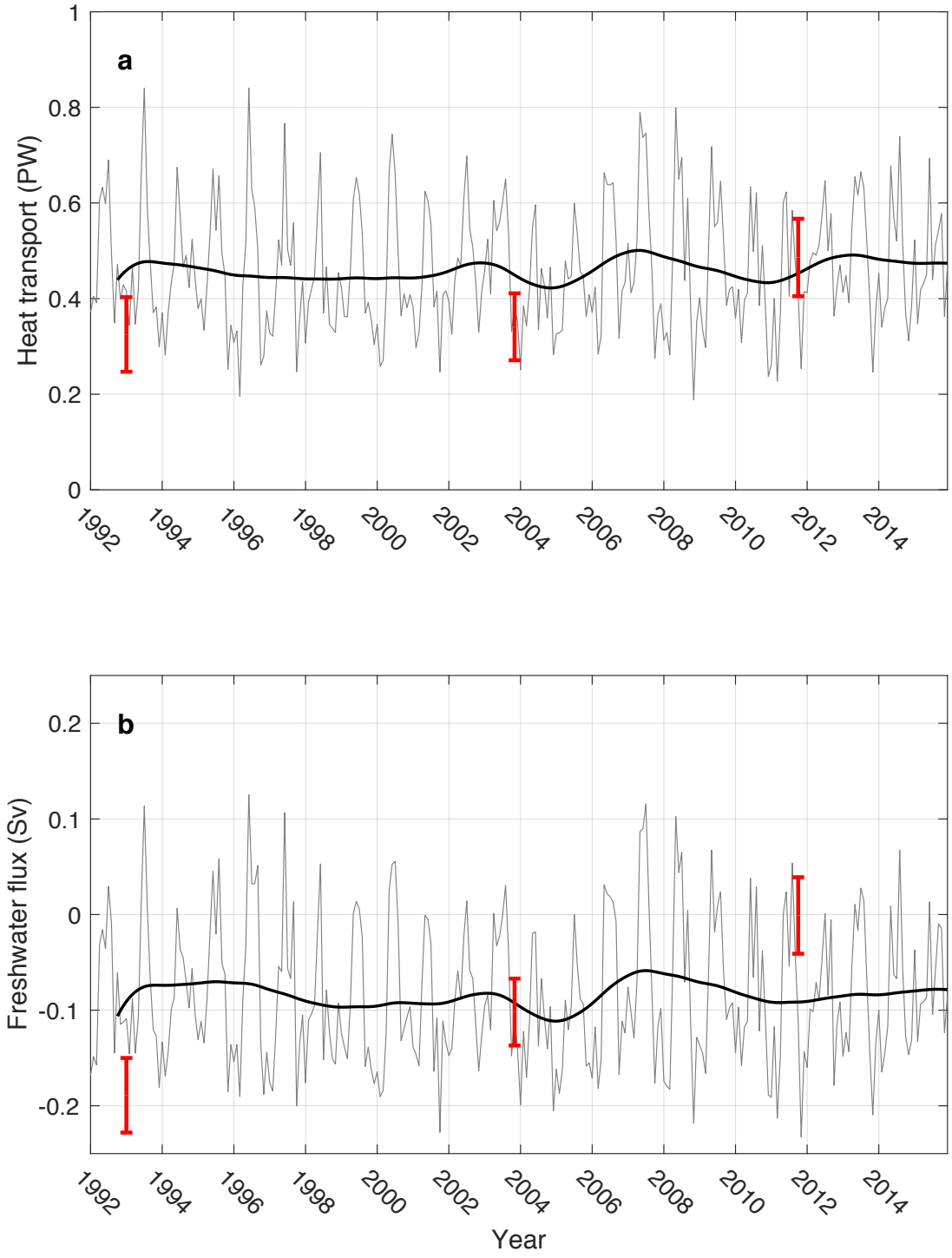

Figure 12. Interannual variability of (a) heat transport (PW) and (b) freshwater flux (Sv) in the South Atlantic at 30ºS for the different months using ECCOv4r3 data for the period 1992-2015 (grey line), with a Butterworth filter (black line) and red error bars to show the values of heat transport and freshwater flux obtained from hydrographic data for the years 1993, 2003 and 2011.

3.5 Atlantic Meridional Overturning Circulation (AMOC)

Figure 13 shows the AMOC in the Atlantic Ocean at 30ºS for ECCOv4r3 data and hydrographic data in January 1993, November 2003 and October 2011. In this figure, the AMOC has been computed from the seafloor to the sea surface. The intensity of the overturning is generally described as the maximum in the overturning stream-function, having northward flow for thermocline and intermediate waters (Kanzow et al., 2007; Koltermann et al., 2011). The resulting overturning stream-function for the first 5 layers (γ^n<27.58 kg/m^3), estimated with ECCOv4r3, presents no significant differences if compared to those from hydrographic data, while evident differences are found in the layers above (γ^n>27.58 kg/m^3).

Figure 14 shows the seasonal and interannual variability of AMOC strength in the Atlantic Ocean at 30ºS. Both figures are generated by using ECCOv4r3 data for the period 1992-2015, but figure 14b also includes AMOC values estimated from hydrographic data for the years 1993, 2003 and 2011 (computed by Ganachaud, 2003 and Hernández-Guerra et al., 2019). As shown in figure 14a, the seasonal variability of the AMOC displays a stronger mass transport from April to September (16.6±0.9 Sv), and a weaker mass transport from October to March (14.5±0.2 Sv). The positive values of the AMOC strength shown in figure 14b, indicate a northward flow of warm and salty water in the upper layers of the Atlantic Ocean with ECCOv4r3 data during the period considered herein. Moreover, as seen in table 4, the estimations of AMOC with the ECCOv4r3 model are not significantly different as demonstrated by the comparison with hydrographic data results.

Table 4. AMOC Transport and uncertainty (Sv) for hydrographic data and ECCOv4r3 data in 1993, 2003 and 2011.

	AMOC Transport (Sv)	
Año	**HD**	**ECCO**
1993	18±3	15.1±0.3
2003	13.4±1.3	13.6±0.5
2011	16.3±1.4	15.2±0.9

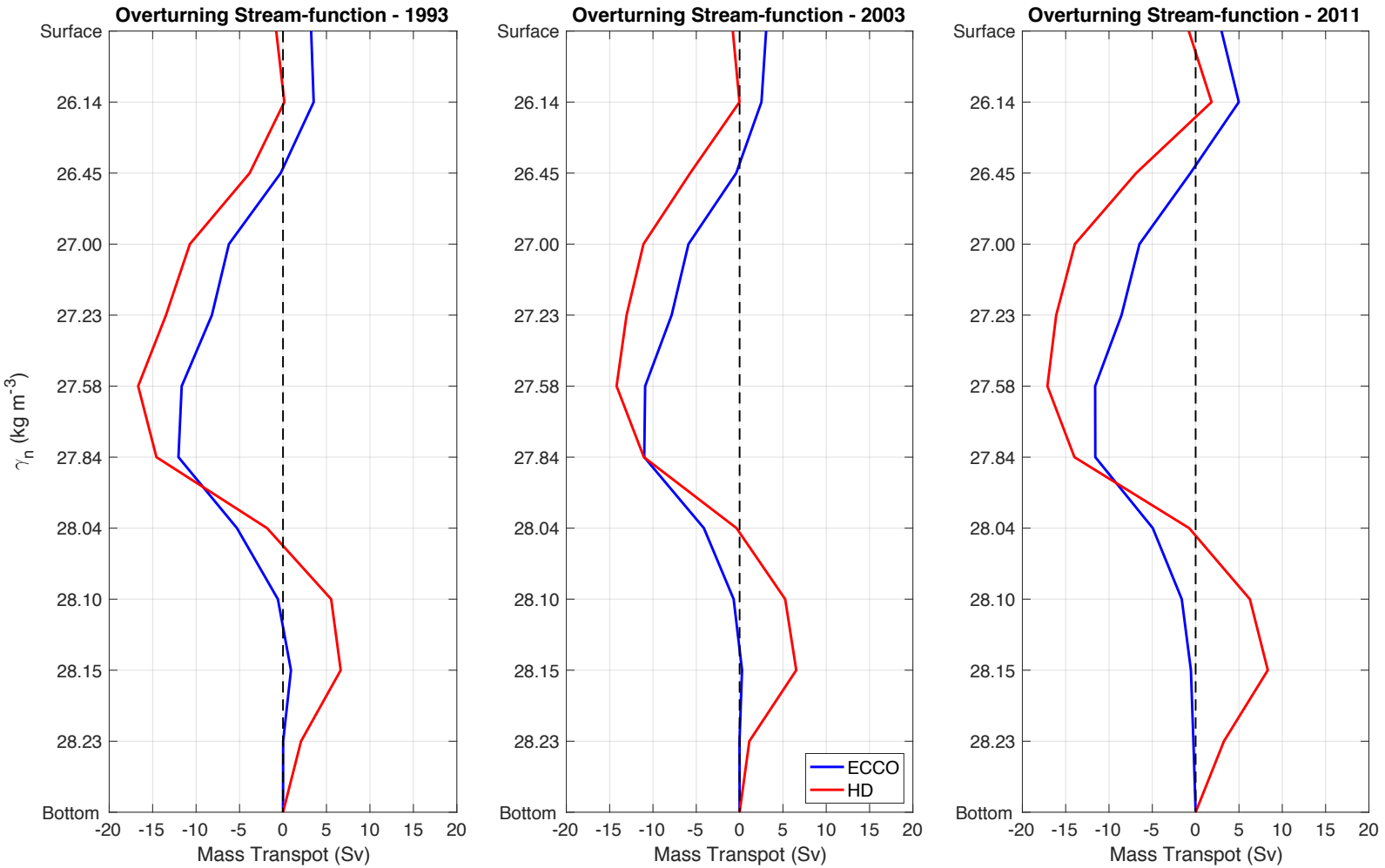

Figure 13. Overturning mass transports in the South Atlantic at 30°S for years 1993, 2003 and 2011. Computed as the zonally- and vertically-integrated mass transports in isoneutral layers, along the entire section from the sea surface to the seafloor for model ECCOv4r3 (blue) and hydrographic data (red).

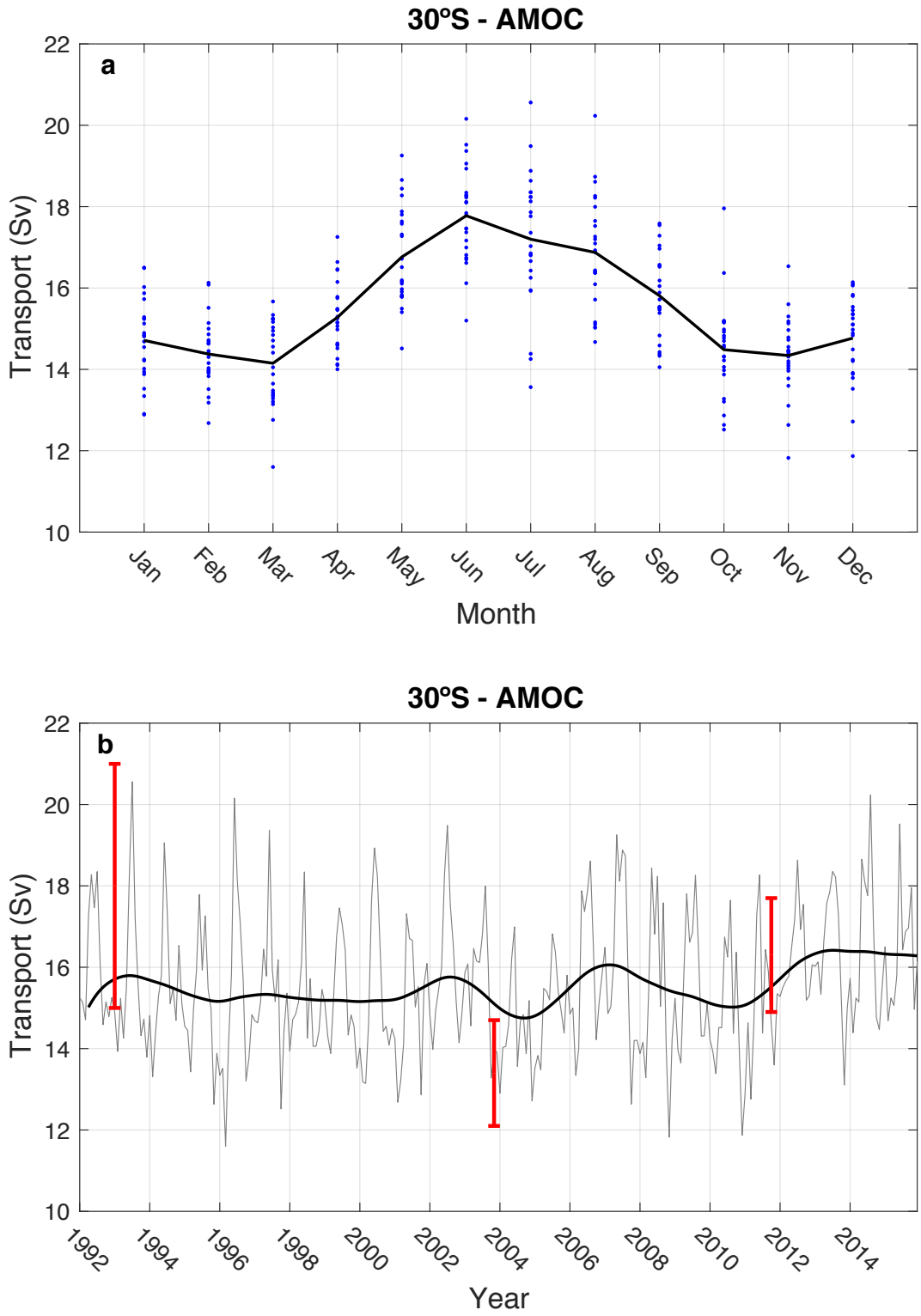

Figure 14. (a) Seasonal variability of the AMOC strength in the Atlantic Ocean at 30ºS using ECCOv4r3 data for the period 1992-2015. For each month, the blue dots correspond to the AMOC for each one of the years in the time period considered herein. The black solid line connects the mean AMOC value of each month, averaged by the different years. (b) Interannual variability of the AMOC strength in the Atlantic Ocean at 30ºS using ECCOv4r3 data for the period 1992-2015. AMOC values using ECCOv4r3 data for the time period of the study are shown by a grey line, the Butterworth filter is shown by a black line and red error bars are used to show the values of the AMOC strength obtained from hydrographic data for the years 1993, 2003 and 2011.

4. DISCUSSION AND CONCLUSION

The ECCOv4r3 model provides monthly data over a 23-year period from January 1992 to December 2015, along 30ºS in the South Atlantic Ocean. The θ/S diagrams present high scattering near the surface of potential temperature and salinity values, regardless of the year. The scattering is higher in 1993, because the data were collected during January, a month characterized by higher solar radiation and temperature, which caused a higher evaporation rate of water from the sea surface. The θ/S diagrams using ECCOv4r3 data, are similar to those obtained from hydrographic data, thus suggesting that the ECCOv4r3 model has not created false water masses and contains all the principal structural characteristics that are persistently and recurrently found in this region.

The estimated water mass transports for the upper layers agree well with the estimations from hydrographic data, since both show a similar value of net northward mass transport, as illustrated in table 1 (1993: HD=18±3 and ECCO=15.1±0.3 Sv; 2003: HD=13.4±0.9 and ECCO=13.6±0.5 Sv; and 2011: HD=16.3±1.4 and 15.2±0.9 Sv). However, the water mass transports in the deep and abyssal layers differ noticeably from the mass transports estimated by hydrographic data. For the deep layers, ECCOv4r3 shows a net southward transport, as hydrographic data do. The net southward mass transports estimated with ECCOv4r3, however, have lower values than those obtained from hydrographic data (1993: HD=-23.3±3 and ECCO=-10.6±0.7 Sv; 2003: HD=-20.7±3.8 and ECCO=-10.2±1.3 Sv; 2011: HD=-25.4±4.2 and ECCO=-10.5±0.8 Sv). The reason is that ECCOv4r3 can model approximately the southward mass transport of the DWBC in the western boundary, but not the southward mass transport of NADW in the eastern boundary. For the abyssal layers, hydrographic data clearly present a net northward mass transport, while ECCOv4r3 does not show this behavior: 1993 (HD=6±1.3 and ECCO=-1.1±0.7 Sv), 2003 (HD=6.5±1.9 and ECCO=-1±0.4 Sv) and 2011 (HD=8.3±2.1 and ECCO=-1.5±0.1 Sv). As a result of the monthly average of the ECCOv4r3 data, the signal of the mesoscale eddies is lost.

The estimation of the seasonal variability of mass transports for the Brazil and Benguela Currents in the Atlantic Ocean at 30ºS, indicate stronger southward mass transport for the Brazil Current from August to March (-15.8±0.8 Sv), than from April to July (-13.3±0.4 Sv); while the mass transport values for the Benguela Current present higher values of northward mass transports from June to November (13.8±0.3 Sv) than from December to May (13.1±0.2). Moreover, the interannual variability of mass

transport for the Brazil (1993: HD=-14±4 and ECCO=-17.8±0.3 Sv; 2003: HD=-25.7±0.7 and ECCO=-15.4±0.04 Sv; 2011: HD=-10.3±0.7 and ECCO=-14.9±0.1 Sv) and Benguela (1993: HD=14±2 and ECCO=12±0.3 Sv; 2003: HD=17.5±0.9 and ECCO=15±0.1 Sv; 2011: HD=12.2±0.8 and ECCO=14.9±0.1 Sv) Currents obtained with ECCOv4r3 are significantly different from the mass transports estimated by hydrographic data, with the exception of 1993.

The seasonal variability of heat transport and freshwater flux in the Atlantic Ocean at 30ºS estimated with the ECCOv4r3 model (Figure 11), shows that there is a northward flux of heat transport, stronger from April to September (0.55±0.07 PW), than from October to March (0.37±0.01 PW). While the seasonal variability of freshwater flux indicates that, in this region, there is higher evaporation than precipitation for almost all year, having higher evaporation from October to March (-0.14±0.01 Sv) than from April to September (-0.03±0.04 Sv). Interestingly, only in June the freshwater flux reaches positive values, caused by higher precipitation than evaporation. Furthermore, the interannual variability estimated with the ECCOv4r3 model suggests that heat transport has similar positive values during the time period considered herein, hence having northward flux of heat transport. Nevertheless, the interannual variability of freshwater flux has similar negative values during the time period considered herein, and not decreasing values as supposed in previously published hydrographic data results. Furthermore, according to the results presented in previous works (Ganachaud, 2003; Hernández-Guerra et al., 2019), the ECCOv4r3 estimations of heat transport (1993: HD= 0.33±0.08 and ECCO=0.42±0.01 PW; 2003: HD=0.34±0.07 and ECCO=0.36±0.04 PW; and 2011: HD=0.49±0.08 and ECCO=0.44±0.05 PW) and freshwater flux (1993: HD=-0.19±0.03 and ECCO=-0.11±0.00 Sv; 2003: HD=-0.10±0.04 and ECCO=-0.13±0.03 Sv; and 2011: HD=-0.00±0.04 and ECCO=-0.08±0.05 Sv) show no significant differences if compared to hydrographic data results, except for the freshwater flux in 1993.

The overturning stream-function is computed by zonally and vertically integrating the mass transport from the seafloor to the sea surface using data obtained from the ECCOv4r3 model. The resulting overturning stream-function is compared from hydrographic data of previous works. This comparison suggests that ECCOv4r3 provides reasonable values for the AMOC. The seasonal variability of the AMOC strength suggests a stronger mass transport from April to September (16.6±0.9 Sv) than from October to March (-0.03±0.04 Sv). The positive values of the AMOC strength, indicate a northward flow of warm and salty water in the upper layers of the Atlantic Ocean with ECCOv4r3

data during the period considered herein. Moreover, the estimations of AMOC with the ECCOv4r3 model are accurate, as demonstrated by the comparison with hydrographic data (1993: HD=18±3 and ECCO=15.1±0.3 Sv; 2003: HD=13.4±1.3 and ECCO=13.6±0.5 Sv; and 2011: HD=16.3±1.4 and 15.2±0.9 Sv). Furthermore, in the outputs of the ECCOv4r3 model, a decrease of the AMOC in 2004 is observed, similarly to the results found by Bryden et al. (2005) with hydrographic data.

By way of conclusion, the solution of ECCOv4r3 is an acceptable fit to most data and has been found to be physically plausible in many aspects for the thermocline and intermediate layers, as demonstrated by the comprehensive analysis performed here. Thus, this model can be used to accurately calculate the different properties of the ocean in the upper layers within a wide period of time. However, the ECCOv4r3 solution for the deep and abyssal layers differs noticeably from the hydrographic data and cannot be used to obtain accurate and representative results.

5. REFERENCES

Bretherton, F. P., Davis, R. E., and Fandry, C. B. (1976). A technique for objective analysis and design of oceanographic instruments applied to MODE-73. *Deep Sea Research*, *23*, 559–582.

Bryden, H. L., Longworth, H. R., and Cunningham, S. A. (2005). Slowing of the Atlantic meridional overturning circulation at 25ºN. *Nature*, *438*, 655–657. https://doi.org/10.1038/nature04385

Chapman, P. (1998). The World Ocean Circulation Experiment (WOCE). *Marine Technology Society Journal*, *32*(3), 23-36.

Cushman-Roisin, B., and Beckers, J. M. (2007). *Introduction to Geophysical Fluid Dynamics*. Academic Press.

Dickson, R. R., and Brown, J. (1994). The production of North Atlantic Deep Water: sources, rates, and pathways. *Journal of Geophysical Research: Oceans*, *99(C6)*, 12319–12341. https://doi.org/10.1029/94JC00530

Forget, G., Campin, J. M., Heimbach, P., Hill, C. N., Ponte, R. M., and Wunsch, C. (2015). ECCO version 4: An integrated framework for non-linear inverse modeling and global ocean state estimation. *Geoscientific Model Development*, *8*(10), 3071–3104. https://doi.org/10.5194/gmd-8-3071-2015

Fukumori, I., Wang, O., Fenty, I., Forget, G., Heimbach, P., and Ponte, R. M. (2017). ECCO Version 4 Release 3. https://doi.org/1721.1/110380

Ganachaud, A. (2003). Large-scale mass transports, water mass formation, and diffusivities estimated from World Ocean Circulation Experiment (WOCE) hydrographic data. *Journal of Geophysical Research: Oceans*, *108(C7)*. https://doi.org/10.1029/2002jc001565

Ganachaud, A., and Wunsch, C. (2003). Large-scale ocean heat and freshwater transports during the World Ocean Circulation Experiment. *Journal of Climate*, *16(4)*, 696–705.

Gordon, A. L. (1981). South Atlantic thermocline ventilation. *Deep Sea Research Part A*. *Oceanographic Research Papers, 28(11)*, 1239–1264.

Gordon, A. L. (1986). Interocean exchange of thermocline water. *Journal of Geophysical Research: Oceans*, *91(C4)*, 5037–5046. https://doi.org/10.1029/JC091iC04p05037

Gordon, A. L. (1989). Brazil-Malvinas Confluence-1984. *Deep Sea Research Part A. Oceanographic Research Papers, 36(3)*, 359–384. https://doi.org/10.1016/0198-0149(89)90042-3

Hernández-Guerra, A., Talley, L. D., Pelegrí, J. L., Vélez-Belchí, P., Baringer, M., Macdonald, A., and McDonagh, E. L. (2019). The Upper, Deep, Abyssal and Overturning Circulation in the Atlantic Ocean at 30ºS in 2003 and 2011 (submitted).

Joyce, T. M., Hernández-Guerra, A., and Smethie, W. M. (2001). Zonal circulation in the NW Atlantic and Caribbean from a meridional World Ocean Circulation Experiment hydrographic section at 66ºW. *Journal of Geophysical Research: Oceans*, *106(C10)*, 22095-22113.

Kanzow, T., Cunningham, S. A., Rayner, D., Hirschi, J. J.-M., Johns, W. E., Baringer, M. O., Bryden, H. L., Beal, L. M., Meinen, C. S., and Marotzke, J. (2007). Observed flow compensation associated with the MOC at 26.5ºN in the Atlantic. *Science*, *317*, 938–941. https://doi.org/10.1126/science.1141304

Koltermann, K. P., Gouretski, V., and Jancke, K. (2011). *Hydrographic Atlas of the World Ocean Circulation Experiment (WOCE): Volume 3: Atlantic Ocean.* National Oceanography Centre. http://doi.org/10.21976/C6RP4Z

Lumpkin, R., and Speer, K. (2007). Global ocean meridional overturning. *Journal of Physical Oceanography*, *37(10)*, 2550–2562. doi:10.1175/JPO3130.1

Macdonald, A. M., and Wunsch, C. (1996). An estimate of global ocean circulation and heat fluxes. *Nature*, *382*, 436–439. https://doi.org/10.1038/382436a0

Pickart, R. S. (1992). Water mass components of the North Atlantic deep western boundary current. *Deep Sea Research*, *39(9)*, 1553–1572.

Smethie, W. M., Fine, R. A., Putzka, A., and Jones, E. P. (2000). Tracing the flow of North Atlantic Deep Water using chloroflurocarbons. *Journal of Geophysical Research: Oceans*, *105(C6)*, 14297–14323.

Sprintall, J., and Tomczak, M. (1993). On the formation of Central Water and thermocline ventilation in the Southern Hemisphere. *Deep Sea Research Part I: Oceanographic Research Papers, 40(4)*, 827–848. https://doi.org/10.1016/0967-0637(93)90074-D

Stramma, L., and England, M. (1999). On the water masses and mean circulation of the South Atlantic Ocean. *Journal of Geophysical Research: Oceans*, *104*, 863–883.

Talley, L. D., and McCartney, M. S. (1982). Distribution and circulation of Labrador Sea water. *Journal of Physical Oceanography*, *12(11)*, 1189–1205.

Talley, L. D. (2008). Freshwater transport estimates and the global overturning circulation: Shallow, deep and throughflow components. *Progress in Oceanography*, *78(4)*, 257–303. doi:10.1016/j.pocean.2008.05.001

Talley, L. D. (2003). Shallow, intermediate, and deep overturning components of the global heat budget. *Journal of Physical Oceanography*, *33(3)*, 530–560.

Talley, L. D., Pickard, G. L., Emery, W. J., and Swift, J. H. (2011). *Descriptive Physical Oceanography: An Introduction* (6th ed.). Elsevier Ltd.

Thiébaux, H. J., and Pedder, M. A. (1987). *Spatial Objective Analysis: with applications in atmospheric science.* Academic Press.

Volkov, D. L., Baringer, M., Smeed, D., Johns, W., and Landerer, F. W. (2019). Teleconnection between the Atlantic Meridional Overturning Circulation and sea level in the Mediterranean Sea. *Journal of Climate*, 32(3), 935–955. https://doi.org/10.1175/JCLI-D-18-0474.1

Wang, O., Fukumori, I., and Fenty, I. (2017). An Overview of ECCO Version 4 Release 3's. ftp://ecco.jpl.nasa.gov/Version4/Release3/doc/v4r3_output_fields.pdf

Wunsch, C. (1996). *The Ocean Circulation Inverse Problem.* Cambridge University Press.

Wunsch, C., and Heimbach, P. (2013). Dynamically and kinematically consistent global ocean circulation and ice state estimates. *International Geophysics*, *103*, 553–579. https://doi.org/10.1016/B978-0-12-391851-2.00021-0

Wunsch, C., Heimbach, P., Ponte, R. M., and Fukumori, I. (2009). The global general circulation of the ocean estimated by the ECCO-Consortium. *Oceanography*, *22(2)*, 88–103. https://doi.org/10.5670/oceanog.2009.41